Observation of the Decay Dynamics and Instabilities of Megagauss Field Structures in Laser-Produced Plasmas

C. K. Li, F. H. Séguin, J. A. Frenje, J. R. Rygg, and R. D. Petrasso
Plasma Science and Fusion Center, Massachusetts Institute of Technology, Cambridge, Massachusetts 02139, USA

R. P. J. Town, P. A. Amendt, S. P. Hatchett, O. L. Landen, A. J. Mackinnon, P. K. Patel, and M. Tabak
Lawrence Livermore National Laboratory, Livermore, California 94550, USA

J. P. Knauer, T. C. Sangster, and V. A. Smalyuk
Laboratory for Laser Energetics, University of Rochester, Rochester, New York 14623, USA
(Received 30 October 2006; published 2 July 2007)

Monoenergetic proton radiography was used to make the first measurements of the long-time-scale dynamics and evolution of megagauss laser-plasma-generated magnetic field structures. While a 1-ns 10^{14} W/cm^2 laser beam is on, the field structure expands in tandem with a hemispherical plasma bubble, maintaining a rigorous 2D cylindrical symmetry. With the laser off, the bubble continues to expand as the field decays; however, the outer field structure becomes distinctly asymmetric, indicating instability. Similarly, localized asymmetry growth in the bubble interior indicates another kind of instability. 2D LASNEX hydrosimulations qualitatively match the *cylindrically averaged* post-laser plasma evolution but even then it underpredicts the field dissipation rate and of course completely misses the 3D asymmetry growth.

DOI: 10.1103/PhysRevLett.99.015001 PACS numbers: 52.38.Fz, 52.50.Jm, 52.70.Nc

The long-term decay or relaxation of dynamical systems is of fundamental importance to diverse physical phenomena, be it a simple oscillator, spin-polarized [1] matter, or a solar flare [2]. Here we report, for the first time, on detailed observations and quantitative images of the decay of megagauss (MG) fields initially generated from a laser beam interacting with a foil. With the laser on and the system driven, the magnetic (B) field maintains, as it expands along the perimeter of a hemispherical plasma bubble, a rigorous degree of cylindrical symmetry [3]. However, when laser drive ends, the B field structure continues to expand and decay but with clear 3 dimensional (3D), but distinctly different, structures emerging both along the edge and in the interior of the bubble. We hypothesize that these symmetry-breaking features, never before seen in any high-energy-density (HED) plasmas [4], are related to different instabilities [5–7] that arise during the decay phase.

In our experiments, monoenergetic 14.7-MeV proton radiography [3] was used to obtain gated images of the field evolution during the laser-driven phase (0–1 ns) and in the post-driven phase (1–3 ns). Because of the novelty of the isotropic, monoenergetic, pulsed source with matched detector, a precise field mapping, via the Lorentz force, is obtained for the duration, and over the entire physical expanse, of the expanding bubble. Using this same technique, we recently reported on the laser-driven phase of these dynamics whereby the field achieves ~0.5 MG intensities [3]. Most other previous work in this field has involved much shorter laser pulses ($\leq$ 10 ps) [8] or ~1 ns laser pulses but with limited diagnostic measurements [9] and has not resulted in the direct observation of any instabilities nor of any quantitative field maps at any time, let alone a sequence of them as presented here.

While the laser is on, the B field is generated primarily via $\nabla n_e \times \nabla T_e$ [10] and is convected outward with the expanding bubble because the field is "frozen in." After the laser turns off, the plasma begins to cool, becoming more collisional and increasingly resistive, thus allowing the field to diffuse relative to the fluid [10]. At these post-driven times, the fluid behavior near the bubble edge can be dominated by field and resistive effects; i.e., the plasma β (the ratio of thermal to field energy) can become smaller than 1. This circumstance gives rise to the possibility of resistive instabilities.

The setup of the experiments, performed at the OMEGA laser facility [11], is illustrated schematically in Fig. 1. B fields were generated through laser-plasma interactions on a plastic (CH) foil by a single laser beam (henceforth called the *interaction beam*) with a wavelength of 0.351 μm,

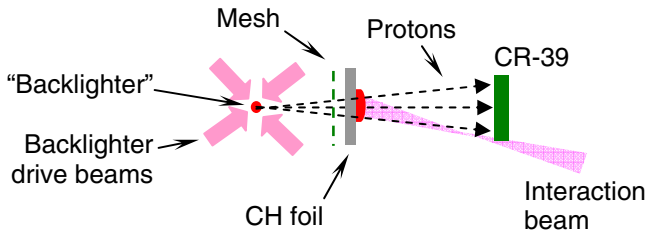

FIG. 1 (color online). Experiment setup. Distances from the backlighter are 1.3 cm for the mesh, 1.5 cm for the CH foil (5 μm thick), and 30 cm for the CR-39 detector.

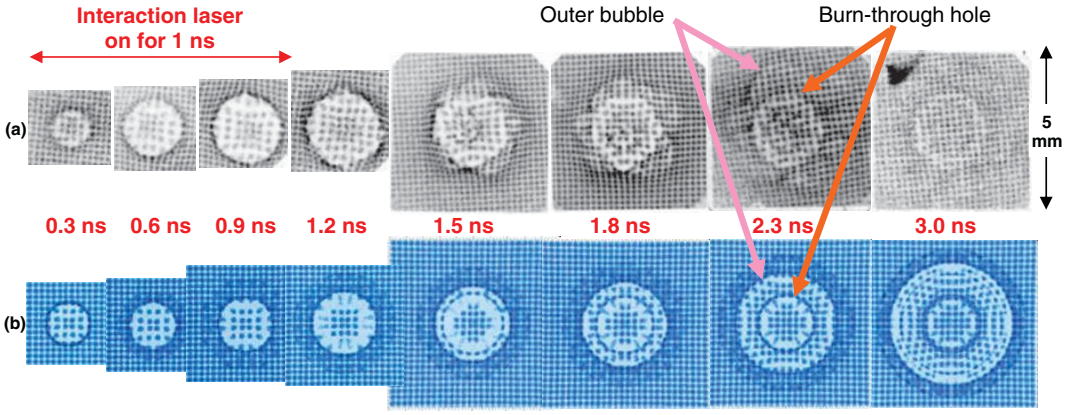

FIG. 2 (color). (a) Measured D^3He proton images showing the evolution of B fields. (b) Corresponding images simulated by LASNEX + LSP. Arrows point to the image features corresponding to fields at the outer bubble boundary and at the laser burnthrough hole shown in Fig. 3(b).

linearly polarized, and incident at 23° from the normal direction. The 1-ns-long square laser pulse had an energy of ~500 J and a spot diameter of 800 μm determined by phase plate SG4 (defined as 95% energy deposition) [12], resulting in a laser intensity of order 10^{14} W/cm^2.

The fields were studied with monoenergetic proton radiography using a backlighter that produced protons isotropically at the discrete energy of 14.7 MeV (fusion products of the nuclear reaction $D + {}^3He \rightarrow \alpha + p$, generated from D^3He-filled, exploding-pusher implosions driven by 20 OMEGA laser beams) [3]. A nickel mesh (60 μm thick with a 150-μm hole-to-hole spacing and 75-μm holes) was used to divide the backlighter protons into discrete beamlets before they passed through the foil, and radiographs were recorded using CR-39 detectors [13]. The duration of each "exposure," determined by the length of time the backlighter produced protons, was ~150 ps. Since the backlighter-to-foil flight time for the protons was ~0.28 ns, an image representing the state of the field at the foil at time t_a after the onset of the interaction beam was made by starting this beam a time $t_a + 0.28$ ns after the mean backlighter production time. To aid in data interpretation, simulations were performed [14] with the 2D hydrodynamic code LASNEX [15] and hybrid particle-in-cell code LSP [16].

Measured images are shown in Fig. 2(a). Each is labeled with a time that represents the interval between the start of the interaction beam and the arrival of the backlighter protons and shows how the proton beamlets were deflected while passing through the B field [3]. For times when the interaction beam was on, each image has a sharp circular ring where beamlets pile up after passing through the edges of the bubble where the B fields were largest (see Fig. 3). This circle is a magnified image of the bubble edge, because the angular deflection of each beamlet is proportional to $\int \mathbf{B} \times d\ell$ (where $d\ell$ is the differential path length along the proton trajectory) and $\mathbf{B} \times d\ell$ points away from the bubble center. The position of each beamlet at the detector plane is thus displaced by a vector ξ ($\propto \int \mathbf{B} \times d\ell$) relative to where it would have been without a field. Beamlets in the center of each image undergo less deflection, indicating that $\int \mathbf{B} \times d\ell$ is smaller there. These features are reasonably well reproduced by LASNEX + LSP simulations for 0.3 to 0.9 ns [Fig. 2(b)]. Figure 3(a) shows the predicted B field in a plane perpendicular to the foil at 0.6 ns. The protons would travel from left to right in the plane of this field map, and the maximum angular deflections would be for trajectories passing through the bubble edges.

After the interaction laser ends, the simulations continue to generally track the behavior of the real data, though less well. The simulations indicate the presence of two rings,

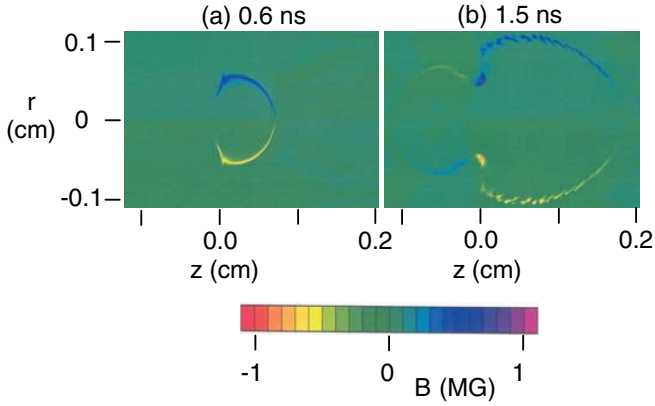

FIG. 3 (color). LASNEX-simulated B field strength on a plane perpendicular to the foil at (a) ~0.6 ns, when the laser was on, and (b) ~1.5 ns, when the laser was off. z is distance from the foil (the laser is incident from the right) and r is distance from the central axis of the plasma bubble. After the laser pulse, strong fields appear near the edge of the hole burned into the foil by the laser, generating the inner circle seen in Fig. 2 for 1.5 ns and later. The simulations predict a second bubble behind the foil after burnthrough, but the simulated images show no feature associated with the field there because it is relatively weak.

the outer one due to the expanding bubble surface, the inner due to fields at the edge of the hole burned through the plastic by the laser (Fig. 2, 1.5–3.0 ns). The data also have these two rings, but the one representing the outer bubble boundary becomes strikingly asymmetric, with 5–10 cycles over the circumference. In addition, the beamlet displacements in the data are much smaller than those in the simulation, indicating that fields have diminished much more quickly than predicted (though both simulation and experiment show a continued expansion of the plasma bubble at late times, leading to convective field dissipation).

These effects can be quantified by measuring the sizes of features in the images and the displacements ξ of individual beamlets seen in the images, because for our truly monoenergetic backlighter there is an exact and unambiguous proportionality between ξ and $\int \mathbf{B} \times d\ell$. The actual bubble size is not the apparent size in the image, because of the magnification referred to above. The true position of the bubble edge is determined by the locations the beamlets in the pileup region would have had in the image if they were not displaced. Sizes determined in this manner are shown in Fig. 4(a), where the radius at late times when the bubble is asymmetric represents an angular average. The bubble radius grows linearly while the laser is on, and then continues to expand after the laser is off. The burnthrough hole radius is also shown in Fig. 4(a). The agreement between data and simulation is, in this averaged sense, quite good for both radii at all times. The amplitudes of the measured asymmetries in the outer bubbles in Fig. 2(a) are plotted in Fig. 4(b). Shown in Fig. 4(c), the peak value occurs at the end of the laser pulse, and it decays thereafter. We note that while the laser is on this maximum occurs at the outside of the bubble, but after the laser is off the maximum occurs at the edge of the burnthrough hole in both data and simulation. The maximum amplitude agrees well for data and simulation, but the data fall off faster than the simulations; this suggests that the actual T_e drops more quickly than in the simulation, enhancing the resistivity and allowing the fields to diffuse and dissipate more quickly.

The net result of the data-simulation comparison is that the 2D code does a reasonable job of predicting the cylindrically ''averaged'' 2D behavior of the bubble and B field generation and expansion, but underestimates the rate of field dissipation and of course does not predict the 3D structure of the asymmetry seen in the data. It might be argued that our observation of 3D structure renders comparison with the 2D simulations irrelevant, but 3D codes are not yet available and it is important to know what can and cannot be predicted with the tools at hand. (Work is currently under way on combining the 3D hydrocode HYDRA with a field generating package [17].) Experimental measurements such as those shown here are important because they directly reveal previously unpredicted

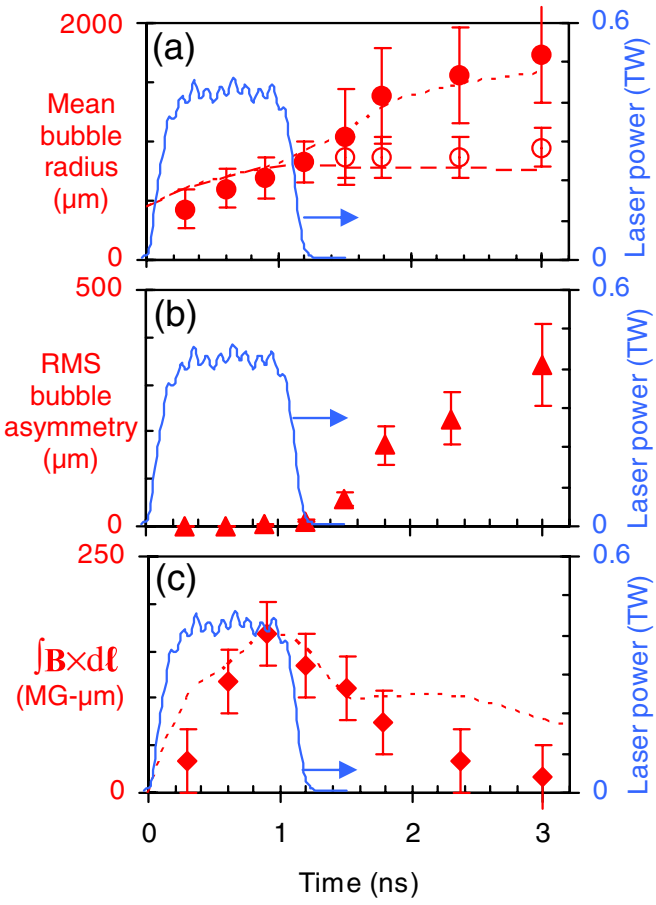

FIG. 4 (color online). (a) Evolution of measured bubble sizes at the foil (solid circles) and at the burnthrough hole (open circles), compared with 2D LASNEX + LSP simulations (dashed lines). The data points represent averages over azimuthal angle. The solid line shows the 1-ns OMEGA laser pulse. (b) rms deviations of the outer bubble boundary from the average radii shown in (a) versus time (this is zero in the simulations). (c) Maximum measured (diamonds) and simulated (dashed line) $|\int \mathbf{B} \times d\ell|$ versus time.

physical phenomena, they indicate the fundamental importance of 3D processes in certain regimes, such as in this decay phase, and they provide invaluable information for benchmarking true 3D code development in the future.

We do not have a complete model for the instability behind the observed periodicity and growth rate of the asymmetry, but the observation itself is new and important. Strong image-to-image similarities in the angular structure of the asymmetry, in spite of the fact that the images are from different shots, must be connected with some constant physical characteristic of the experiment, but the foil has no directional characteristics and the mesh has structure but, in the experiments reported here, is too far (2 mm) behind the foil to be responsible. Furthermore, even changing the mesh distance from 2 to 0.125 mm had no effect on the growth or amplitude of this instability, nor did changing the laser from polarized to unpolarized light.

This is the first observation of such an instability in laser-produced HED plasmas. It is plausible that this is a pressure-driven, resistive magnetohydrodynamic (MHD) interchange instability [6], resulting in an interchange of field between the inside and outside of the bubble surface. It occurs under circumstances such as we have here, with unfavorable field curvature ($\boldsymbol{\kappa} \cdot \boldsymbol{\nabla} p > 0$, where $\boldsymbol{\kappa} = \mathbf{B} \cdot \boldsymbol{\nabla} \mathbf{B}/B^2$ is the field-line curvature and $\boldsymbol{\nabla} p$ is the pressure gradient) and when resistivity allows for radial diffusion of B field into the region outside the bubble. It makes sense that this instability would occur only after the laser is off, as shown in Fig. 4(b), when the cooling plasma becomes more resistive. Of course, we cannot, without additional experiments, completely rule out the possible role of other MHD instabilities, such as kink or tearing modes [6], but they seem less likely to have the observed spatial configuration. Pure fluid instabilities such as the Widnall type [18], on the other hand, might be expected to be visible while the laser is on (when B fields do not have much impact on the flow but are frozen in), but we do not see any evidence for the instability then.

Another type of instability is apparent during the interval from 1.5 to 2.3 ns, where the distributions of beamlets near the image centers have some chaotic structure (different in each image). We noted in earlier work [3] that qualitatively similar chaotic structures occur while the laser is on only if laser phase plates were not used; the phase plates either prevented the chaotic structure from forming as long as the laser was on, or reduced its amplitude sufficiently that it was not visible until it had a chance to grow over a longer time period. In the case at hand, we conjecture that, as the plasma cools and becomes increasingly resistive, an electron thermal instability is triggered and, driven by the heat flow, leads to random filamentary structure of n_e and T_e, as well as B fields [19]. Such instability occurs only in the center region where the mean free path, λ_{mfp}, is smaller than the electron collisionless skin depth $c\omega_{pe}^{-1}$, i.e. $\lambda_{\mathrm{mfp}}/c\omega_{pe}^{-1} \sim (\omega_{ce}\tau L_{\parallel}/L_{\perp})^{1/2} < 1$, where $\omega_{ce}\tau$ is the Hall parameter, $L_{\parallel}$ and $L_{\perp}$ are parallel and perpendicular scale lengths, respectively.

We measured the decay dynamics of laser-plasma-generated MG fields with unprecedented detail and accuracy, making the first observations of asymmetric instabilities in the post-driven phase when resistivity increased due to plasma cooling. 2D LASNEX simulations underestimate the field dissipation rate, in addition to not predicting the 3D instabilities, showing the need for 3D hydro capabilities that include field generating capabilities [17]. Finally, the observations potentially open new areas of research in HED physics, including monoenergetic particle probing of warm dense matter and backlighting of implosions and laboratory astrophysical experiments with the aim of characterizing areal density and fields.

The work described here was performed in part at the LLE National Laser User's Facility (NLUF), and was supported in part by U.S. DOE (Grant No. DE-FG03-03SF22691), LLNL (subcontract Grant No. B504974), and LLE (subcontract Grant No. 412160-001G).

[1] P. Herczeg *et al.*, *Physics Beyond the Standard Model* (World Scientific, Singapore, 1999).
[2] R. D. Petrasso *et al.*, Sol. Phys. **62**, 133 (1979).
[3] C. K. Li *et al.*, Phys. Rev. Lett. **97**, 135003 (2006).
[4] R. C. Davidson, *Frontiers in High Energy Density Physics* (National Academies Press, Washington, DC, 2003).
[5] B. B. Kadomstev, *Review of Plasma Physics* (Consultants Bureau, New York, 1966).
[6] J. P. Freidberg, *Ideal Magnetohydrodynamics* (Plenum, New York, 1987).
[7] M. G. Haines, Phys. Rev. Lett. **78**, 254 (1997).
[8] J. A. Stamper *et al.*, Phys. Rev. Lett. **26**, 1012 (1971); M. Borghesi *et al.*, *ibid.* **81**, 112 (1998); A. J. Mackinnon *et al.*, Rev. Sci. Instrum. **75**, 3531 (2004).
[9] M. G. Drouet *et al.*, Phys. Rev. Lett. **36**, 591 (1976); M. A. Yates *et al.*, *ibid.* **49**, 1702 (1982).
[10] S. Eliezer, *The Interaction of High-Power Lasers with Plasmas* (IOP, Bristol, 2002).
[11] T. R. Boehly *et al.*, Opt. Commun. **133**, 495 (1997).
[12] T. J. Kessler *et al.*, *Laser Coherence Control: Technology and Applications* (SPIE, Bellingham WA, 1993).
[13] F. H. Séguin *et al.*, Rev. Sci. Instrum. **75**, 3520 (2004).
[14] R. P. J. Town *et al.*, Bull. Am. Phys. Soc. **51**, 142 (2006).
[15] G. B. Zimmerman and W. L. Kruer, Comments Plasma Phys. Control. Fusion **2**, 51 (1975).
[16] D. R. Welch *et al.*, Nucl. Instrum. Methods Phys. Res., Sect. A **464**, 134 (2001).
[17] M. M. Marinak (private communication).
[18] S. E. Widnall *et al.*, J. Fluid Mech. **66**, 35 (1974).
[19] M. G. Haines, Phys. Rev. Lett. **47**, 917 (1981).